Journal of Catalysis 272 (2010) 131–139

Contents lists available at ScienceDirect

Journal of Catalysis

journal homepage: www.elsevier.com/locate/jcat

Quantitative solid-state NMR investigation of V^{5+} species in VPO catalysts upon sequential selective oxidation of *n*-butane

Jörg Frey [a], Christian Lieder [a], Thomas Schölkopf [b], Thomas Schleid [b], Ulrich Nieken [c], Elias Klemm [a], Michael Hunger [a,*]

[a] Institute of Chemical Technology, University of Stuttgart, 70550 Stuttgart, Germany
[b] Institute of Inorganic Chemistry, University of Stuttgart, 70550 Stuttgart, Germany
[c] Institute for Chemical Process Engineering, University of Stuttgart, 70199 Stuttgart, Germany

ARTICLE INFO

Article history:
Received 13 January 2010
Revised 2 March 2010
Accepted 3 March 2010
Available online 8 April 2010

Keywords:
Selective *n*-butane oxidation
VPO catalysts
Mars–van-Krevelen mechanism
V^{5+} species
Solid-state NMR spectroscopy

ABSTRACT

Bulk VPO catalysts (VPO/bulk) and VPO catalysts supported on mesoporous SBA-15 material (VPO/SBA-15) were treated sequentially in a flow of nitrogen loaded with *n*-butane and of synthetic air loaded with *n*-butane in order to reach a complete reduction and reoxidation, respectively, of the catalyst surface. The V^{5+} species on these VPO catalysts were quantitatively investigated by solid-state NMR spectroscopy and correlated with the catalytic activities of the corresponding materials in the selective oxidation of *n*-butane to maleic anhydride. By $^{31}P\{^1H\}$ cross-polarization MAS NMR experiments on the *n*-butane-loaded VPO/SBA-15 catalyst was evidenced that *n*-butane is preferentially adsorbed at surface sites of δ-$VOPO_4$-like phases. Based on the number of P/V^{5+} species in δ-$VOPO_4$-like phases as determined by MAS NMR spectroscopy, the turnover frequency of the surface sites on the VPO/SBA-15 catalyst was estimated to be about 0.2 s^{-1}.

1. Introduction

Vanadium phosphate (VPO) materials belong to the most complex catalysts in heterogeneous catalysis. VPO catalysts are industrially applied in the selective oxidation of *n*-butane to maleic anhydride (MA) comprising the stepwise abstraction of eight hydrogen atoms leading to the formation of four water molecules and the insertion of three oxygen atoms. Until now, there is a controversy discussion on the composition of the highly active VPO catalysts and the nature of their active surface sites [1]. It is widely assumed that vanadyl pyrophosphate $(VO)_2P_2O_7$ is the main component of the bulk VPO catalysts, which are covered with defect sites or other amorphous and crystalline vanadyl phosphate phases [2–6]. Recent studies focusing on the investigation of the surface structure and composition of VPO materials indicated that the surface regions of the catalyst particles are very different from the bulk phase [7–11]. Applying Raman spectroscopy, XPS, and EXAFS techniques, various orthophosphates, such as members of the δ-$VOPO_4$ family, could be indentified on vanadyl pyrophosphate particles, which are involved in redox and oxidation cycles [7,11]. In contrast to the vanadyl pyrophosphate built by vanadium atoms in the oxidation state +4 (V^{4+}), vanadyl orthophosphates consist of vanadium atoms in the oxidation state +5 (V^{5+}).

Generally, VPO catalysts are prepared *via* an *in situ* activation of vanadyl hydrogenphosphate hemihydrate $VOHPO_4{\cdot}0.5H_2O$ in a flow of air loaded with *n*-butane [1]. This procedure leads to VPO catalysts composed of vanadyl pyrophosphate and vanadyl orthophosphate phases, such as α_I-, α_{II}-, β-, γ-, δ-$VOPO_4$ [1,12–15]. Furthermore, a reversible transformation of orthophosphate phases into the vanadyl pyrophosphate is discussed, which corresponds to a change of the oxidation state of vanadium atoms from the V^{5+} to the V^{4+} state and, possibly, to the V^{3+} state and *vice versa* [15]. The change, e.g., between the V^{5+} and V^{4+} states is accompanied by a release of oxygen atoms from the catalyst framework and their transfer to reactant molecules. The formed framework vacancies are filled by oxygen from the gas phase changing the oxidation state of the framework vanadium back from V^{4+} to V^{5+}. This catalytic cycle corresponds to the Mars–van-Krevelen mechanism [16].

Since V^{4+} and V^{3+} species are paramagnetic, they are not accessible for solid-state NMR spectroscopy in a direct manner. However, static ^{31}P spin-echo NMR spectroscopy allows the separation of signals due to phosphorus atoms in the proximity of V^{5+} (−40 to 10 ppm), V^{4+} (very broad signal at *ca.* 2500 ppm), and V^{3+} species (very broad signal at *ca.* 4650 ppm) in VPO compounds [17–19]. Magnetic susceptibility measurements of vanadyl pyrophosphate confirmed the presence of paramagnetic V^{4+} species in this material. Li et al. [17] found that the observed ^{31}P NMR shifts of up to 2500 ppm for phosphorus atoms in the proximity of paramagnetic V^{4+} species are due to electron-nuclear

* Corresponding author. Fax: +49 711 68564081.
E-mail address: michael.hunger@itc.uni-stuttgart.de (M. Hunger).

0021-9517/$ - see front matter © 2010 Elsevier Inc. All rights reserved.
doi:10.1016/j.jcat.2010.03.004

dipolar-plus-contact interactions, which also cause the strong line broadenings of the ^{31}P NMR signals of up to 1000 ppm. In contrast, phosphorus atoms in the proximity of diamagnetic V^{5+} species (P/V^{5+}) and V^{5+} species themselves have been successfully investigated by high-resolution ^{31}P and ^{51}V MAS NMR spectroscopy (MAS: magic angle spinning), respectively [20–24]. In these cases, the residual line width of the ^{31}P and ^{51}V MAS NMR signals mainly depends on the distribution of bond distances and angles in the local structure of the resonating nuclei.

In the present study, the sensitivity of solid-state NMR spectroscopy for local structures and the quantitative character of this method were utilized for, to the best of our knowledge, first quantitative investigation of P/V^{5+} species in differently treated VPO catalysts. For these studies, VPO catalysts were treated under reaction conditions in such a manner that the number of catalytically active V^{5+} atoms was decreased by reduction in a flow of nitrogen loaded with *n*-butane and increased in a flow of synthetic air loaded with *n*-butane. The MAS NMR experiments focused on the separation and quantification of P/V^{5+} species and the assignment of the corresponding vanadyl orthophosphate phases after transfer of the spent catalysts into MAS NMR rotors. To enhance the sensitivity of the MAS NMR spectroscopy for the catalytically interesting P/V^{5+} sites, the VPO compounds were dispersed on mesoporous SBA-15 material acting as a catalyst support. For the obtained VPO/SBA-15 material, a significantly higher specific surface area of the VPO compounds in comparison with VPO/bulk catalysts could be expected [25,26].

2. Experimental

2.1. Materials

The bulk VPO catalyst (VPO/bulk) used as reference material was prepared *via* vanadyl hydrogenphosphate hemihydrate ($VOHPO_4{\cdot}0.5H_2O$). This precursor was obtained according to the following standard procedure [27,28]: 1.46 g V_2O_5 and 2.21 g 85% H_3PO_4 were given in 29-ml isobutanol and 2.9-ml benzyl alcohol. The synthesis was carried out at 373 K for 6 h in a 250-ml round bottom flask equipped with a stirrer and reflux condenser. After completion of the reaction, the precipitate was recovered by filtration, thoroughly washed in acetone and demineralised water, and dried in synthetic air at 393 K for 12 h leading to the blue vanadyl hydrogenphosphate hemihydrate precursor. By ICP-AES, the phosphorus to vanadium ratio of the precursor was determined to 1.01.

The synthesis of the SBA-15 material used as catalyst support was performed as described by Zhao et al. [29]: 6.0 g of the triblock copolymer P123 (Aldrich) was added to 29.4 g of HCl (37%) and 192 g deionised water until all the P123 was dissolved. Subsequently, this mixture was dropwise added to 13.2 g tetraethylorthosilicate (Aldrich, 98%) and vigorously stirred for 10 min. At first, the mixture was heated at 313 K for 24 h and, upon transfer into a Teflon-lined 200-ml autoclave, at 373 K for another 24 h. After cooling to room temperature, the solid product was washed with deionised water and dried in air at 353 K overnight. For decomposing the templates, the as-synthesized material was heated with a rate of 2 K min^{-1} up to 823 K and calcined at this temperature in synthetic air for 5 h.

For the preparation of the SBA-15-supported VPO catalyst (VPO/SBA-15 with 60 wt.% VPO), the synthesis of the vanadyl hydrogenphosphate hemihydrate precursor $VOHPO_4{\cdot}0.5H_2O$ was performed according to Li et al. [25,26]: 0.54 g of V_2O_5 was refluxed at 413 K for 5 h in a mixture of isobutanol and benzyl alcohol (10 ml each). Then, 0.524 g of polyethyleneglycol 6000 (PEG 6000 by Fluka) and 0.90 g of the calcined SBA-15 material were added accordingly. After 1 h, 0.274 g of 85% H_3PO_4 was added dropwise to the mixture. This mixture was allowed to reflux for 6 h before the suspension was filtered, and the solid was washed with isobutanol and acetone. The solid was dried in synthetic air at 393 K for 12 h. By ICP-AES, the phosphorus to vanadium ratio of the VPO/SBA-15 material was determined to 1.04.

The activation of the VPO/bulk and VPO/SBA-15 catalysts under study was carried out under a gas flow of 98.5 ml synthetic air and 1.5 ml *n*-butane per minute by heating with a rate of 2 K min^{-1} from room temperature to 678 K. This temperature was kept for 24 h under the above-mentioned gas flow.

2.2. Characterization techniques

The activated catalysts were characterized by chemical analysis (ICP-AES, Varian Vista-MPX) and X-ray diffraction (Bruker D8 ADVANCE, Cu Kα radiation). Nitrogen adsorption was carried out at a Quantachrom Autosorb 1C upon degassing the samples at 573 K for 3 h. Then, the adsorption was conducted at 77 K. SEM pictures were recorded at a Cambridge CamScan 44 scanning electron microscope for studying the morphology of the materials.

The selective oxidation of *n*-butane on the catalysts under study was investigated using a fixed-bed laboratory reactor with a bed diameter and bed height of each 10 mm, the feed rate of 100 ml min^{-1} with compositions of 98.5 vol.% synthetic air and 1.5 vol.% *n*-butane under atmospheric pressure, and at the reaction temperature of 678 K. The reactor was charged with 500 mg of the catalyst precursor crushed and sieved to particles of 200–315 μm. The reaction products were analyzed by an *on-line* gas chromatograph HP 6890 equipped with a column HP-5 (length 30 m). Before the catalytic experiments, the catalysts were activated at 678 K for 24 h as described in Section 2.1. The end of this activation procedure defined the starting point of the sequential catalytic experiments. In these sequential experiments, an oxidizing feed consisting of synthetic air loaded with *n*-butane (1.5 vol.%) was introduced into the reactor for 20 min before the feed was switched to a reducing gas mixture consisting of nitrogen loaded with *n*-butane (1.5 vol.%) for 40 min and so on.

For the *on-line* study of the oxidation state of the vanadium in the VPO catalysts, the fixed-bed laboratory reactor was equipped with a high-temperature glass-fiber reflection probe HPSUV1000A by Oxford-Electronics connected with a fiber-optic spectrometer AvaSpec-2048 and an AvaLight-DH-S light source by Avantes. The window of the reflection probe was fixed *ca.* 1 mm over the catalyst bed (see Refs. [30,31]). With this technique, the absorbance of the UV/Vis charge-transfer (between O^{2-} and V^{5+}) band at *ca.* 400 nm, characteristic for vanadium species in the oxidation state +5 (V^{5+}), was detected [32]. The evaluation of the band intensity was performed according to the Kubelka–Munk function [33].

^{31}P and ^{51}V MAS NMR investigations were performed on a Bruker MSL-400 spectrometer at resonance frequencies of 161.98 and 105.25 MHz, with repetition times of 30 and 0.5 s, and with 4.800 and *ca.* 100.000 scans per spectrum, respectively. ^{31}P and ^{51}V nuclei were studied using 4 mm and 2.5 mm MAS NMR rotors with spinning rates of 8 kHz and 12.5–20.0 kHz, respectively. The quantitative ^{31}P MAS NMR studies of the number of phosphorous atoms in the proximity of V^{5+} species (P/V^{5+}) were carried out by comparing the signal intensities of the catalyst samples with that of an external intensity standard recorded with a repetition time of 120 s. This intensity standard consisted of a well-characterized silicoaluminophosphate SAPO-34 diluted with SBA-15 in a ratio of 1:4 [34]. For the $^{31}P\{^1H\}$ cross-polarization MAS NMR experiments, a contact pulse of 5 ms and a repetition time of 2 s were used.

Before the XRD and solid-state NMR characterization of the activated, reduced, and reoxidized catalyst samples, the corresponding materials were transferred from the fixed-bed laboratory reactor to the XRD sample carriers and into the MAS NMR rotors

without contact to air in a glove box purged with dry nitrogen gas. After the above-mentioned transfer, the XRD sample supports were covered and sealed by a gas-tight foil, and the MAS NMR rotors were sealed with gas-tight caps.

3. Results and discussion

3.1. Characterization of the materials under study

In Fig. 1, the SEM pictures of the calcined VPO/bulk and VPO/SBA-15 catalysts (a and c) and the calcined SBA-15 material (b) are shown. In contrast to the images of α_I-, α_{II}-, β-, γ-, and δ-$VOPO_4$ standard phases with large plate-like morphologies [14], the VPO/bulk catalyst used in the present study consists of small rectangular-shaped crystallites with a diameter of *ca.* 1 μm, which are agglomerated to form large particulates (Fig. 1a). This morphology is very similar to that described by Kiely et al. [14] for $(VO)_2P_2O_7$ crystallites. The image of the pure SBA-15 material used as catalyst support shows rope-like particles with uniform diameters of *ca.* 1 μm (Fig. 1b). After loading this SBA-15 material with the vanadyl hydrogenphosphate hemihydrate precursor and subsequent calcination (Fig. 1c), the sample consists of broken rope-like particles and particles similar to $(VO)_2P_2O_7$ crystallites. This observation hints to the presence of SBA-15 covered by VPO compounds. This explanation agrees with the significant decrease in the number of SiOH groups of the SBA-15 materials upon loading with VPO compounds as recently demonstrated by ^1H and ^{29}Si MAS NMR investigations of VPO/SBA-15 materials in an earlier study [24].

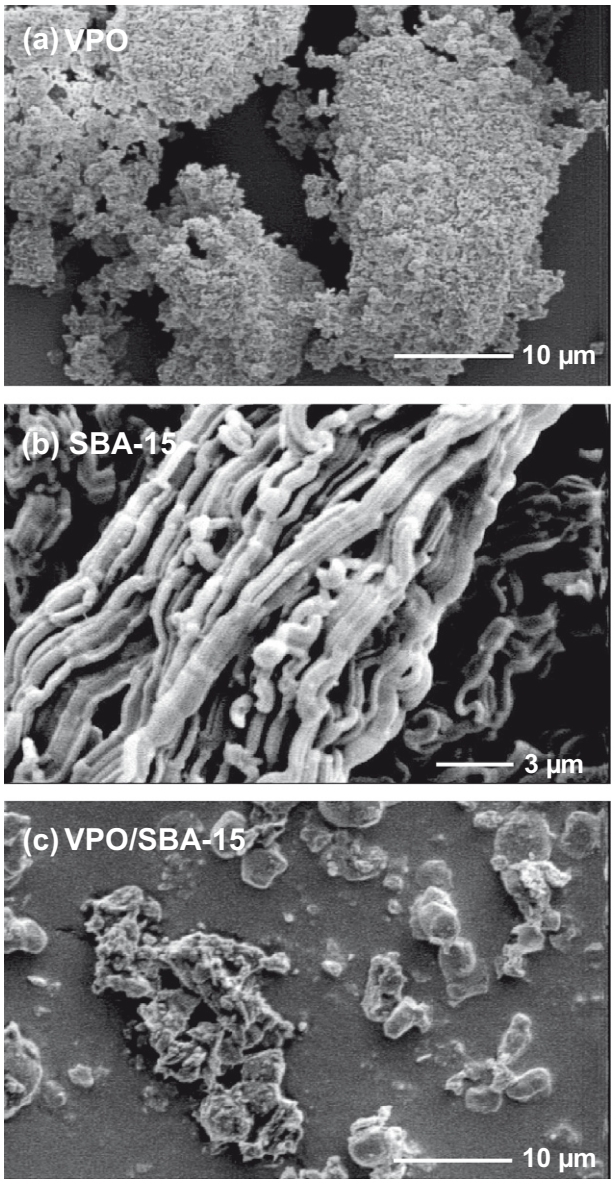

Fig. 1. SEM pictures of the calcined VPO/bulk catalyst (a), the calcined SBA-15 material (b), and the calcined VPO/SBA-15 catalyst (c). Calcination of VPO/bulk and VPO/SBA-15 was performed at 678 K for 24 h in synthetic air loaded with 1.5 vol.% *n*-butane, while calcination of the SBA-15 material was carried out in synthetic air at 823 K for 5 h.

The results of nitrogen adsorption on the calcined VPO/bulk, SBA-15, and VPO/SBA-15 samples are summarized in Table 1. The BET surface area of the VPO/bulk catalyst of 13 $m^2\,g^{-1}$ lies in the typical range of 2–43 $m^2\,g^{-1}$ described for calcined bulk VPO catalysts in literature [14,28]. For calcined VPO catalysts prepared *via* the alcohol solution route, like used in the present work, Kiely et al. [14] obtained a specific surface area of 14 $m^2\,g^{-1}$. The specific surface area of 1164 $m^2\,g^{-1}$ determined for the calcined SBA-15 material before loading with VPO compounds and the mesopore size of 60 Å are typical for this mesoporous structure [25,26,29]. Loading of the SBA-15 material with the vanadyl hydrogenphosphate hemihydrate precursor led to a decrease of the specific surface area from 1164 to 456 $m^2\,g^{-1}$ and of the mesopore diameter from 60 to 48 Å. These data and the significant decrease of the SiOH groups upon loading of SBA-15 with the vanadyl hydrogenphosphate hemihydrate precursor and subsequent calcination indicate that the external and internal surfaces of the SBA-15 particles in the VPO/SBA-15 material are directly covered by VPO compounds. In connection with the dispersion of the VPO compounds on the SBA-15 support, an increased specific surface area of the catalytically active species is expected, which is advantageous for the further spectroscopic investigations due to the larger number of surface sites.

The XRD patterns of the activated VPO/bulk and VPO/SBA-15 catalysts, composed of the reflections of vanadyl pyrophosphate and orthophosphates, are discussed in detail in Section 3.3.

3.2. Catalytic and UV/Vis characterization of VPO/bulk and VPO/SBA-15 catalysts during the selective oxidation of n-butane

The catalytic data obtained after reaching the steady state in the fixed-bed laboratory reactor, *i.e.*, upon the reaction time of 24 h, are summarized in Table 2. These data obtained for the selective oxidation of *n*-butane at 678 K with the total feed rate of 100 ml min^{-1} and 1.5 vol.% *n*-butane indicate that the VPO/SBA-15 catalyst is as active as the VPO/bulk catalyst.

The further catalytic experiments focused on the preparation of VPO catalysts with different oxidation states of the vanadium species within a reasonable experiment time and in a reversible manner. Therefore, after the activation of the VPO catalysts in a feed consisting of synthetic air loaded with *n*-butane, the oxygen in the gas flow was switched off and on for reaching a complete reduction and reoxidation of the catalyst surface (see Figs. 2 and 3). Using 500 mg VPO catalyst in a fixed-bed laboratory reactor

Table 1
Nitrogen adsorption data of the calcined VPO/bulk catalyst, the calcined SBA-15 material, and the calcined VPO/SBA-15 catalyst.

Material	BET surface area ($m^2\,g^{-1}$)	Mesopore size (Å)	Mesopore volume ($cm^3\,g^{-1}$)
VPO/bulk	13	250	0.08
SBA-15	1164	60	1.25
VPO/SBA-15	456	48	0.54

with the bed diameter and bed height of 10 mm and the total feed rate of 100 ml min^{-1} nitrogen loaded with 1.5 vol.% *n*-butane, a reduction period (assigned in Figs. 2 and 3 with 'no O_2') of 40 min led to a total decline of the MA yield. A period of 20 min using the total feed rate of 100 ml min^{-1} synthetic air loaded with 1.5 vol.% *n*-butane was necessary for the complete reoxidation (assigned 'O_2') of the VPO catalysts. With this sequential reaction procedure, a reproducible reduction and reoxidation of the VPO/bulk and VPO/SBA-15 catalysts was reached. Within an experimental accuracy of ±1%, the conversion *X* of *n*-butane, the selectivity *S* to maleic anhydride as well as the yield *Y* to maleic anhydride were stable at the end of each reoxidation period over the whole time-of-stream (see Figs. 2 and 3).

Table 2
Conversion *X* of *n*-butane and selectivity *S* to maleic anhydride (MA) obtained on 500 mg of VPO/bulk and VPO/SBA-15 catalysts at the reaction temperature of 678 K upon activation for 24 h and for the total feed rate of 100 ml min^{-1} synthetic air loaded with 1.5 vol.% *n*-butane.

Material	Conversion *X* of *n*-butane (%)	Selectivity *S* to MA (%)
VPO/bulk	36 ± 2	54 ± 2
VPO/SBA-15	36 ± 2	45 ± 2

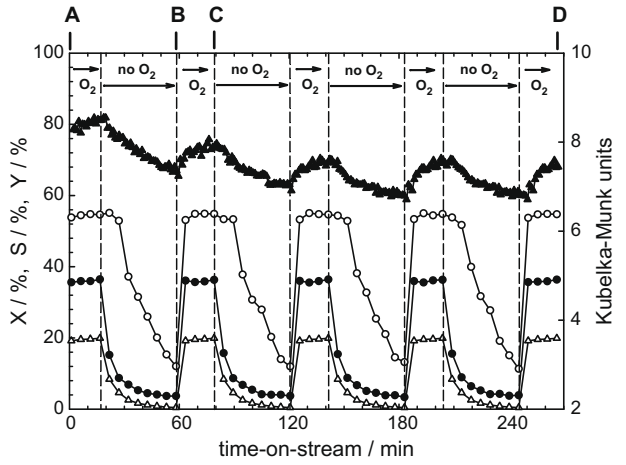

Fig. 2. Conversion *X* of *n*-butane (●), selectivity *S* to maleic anhydride (○), yield *Y* of maleic anhydride (△), and UV/Vis absorption at *ca.* 400 nm (▲), evaluated according to the Kubelka–Munk function, for catalysis on the VPO/bulk catalyst performed at 678 K and using a feed of synthetic air loaded with *n*-butane (periods assigned 'O_2') or nitrogen loaded with *n*-butane (periods assigned 'no O_2'). At the points assigned A–D, samples were taken for the XRD and solid-state NMR investigations.

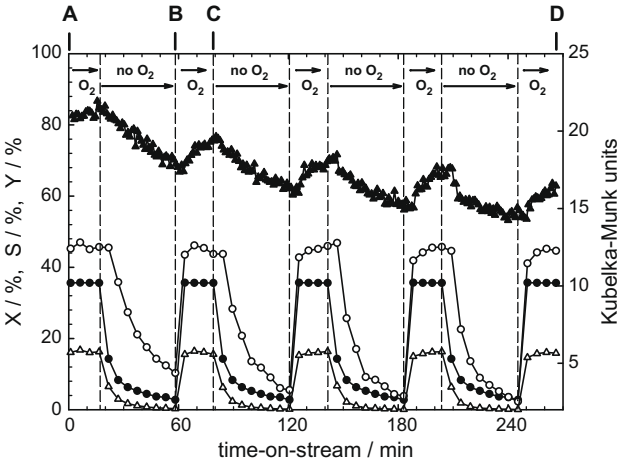

Fig. 3. Conversion *X* of *n*-butane (●), selectivity *S* to maleic anhydride (○), yield *Y* of maleic anhydride (△), and UV/Vis absorption at *ca.* 400 nm (▲), evaluated according to the Kubelka–Munk function, for catalysis on the VPO/SBA-15 catalyst performed at 678 K and using a feed of synthetic air loaded with *n*-butane (periods assigned 'O_2') or nitrogen loaded with *n*-butane (periods assigned 'no O_2'). At the points assigned A–D, samples were taken for the XRD and solid-state NMR investigations.

During the sequential reduction and reoxidation of the VPO catalysts in the fixed-bed laboratory reactor, the change of the oxidation state of vanadium species was observed *on-line* by fiber-optic UV/Vis spectroscopy. In Figs. 2 and 3, top, the intensities of the UV/Vis band of V^{5+} species at *ca.* 400 nm, evaluated according to the Kubelka–Munk function, are plotted. While the reduction of the VPO catalysts (assigned 'no O_2') was always accompanied by a significant decrease of the UV/Vis band at *ca.* 400 nm, the reoxidation (assigned 'O_2') led to an increase of this band. This finding indicates the transformation of V^{5+} into V^{4+} or V^{3+} species and of V^{4+} or V^{3+} into V^{5+} species, respectively. As also observed during selective oxidation of *n*-butane under continuous flow of *n*-butane and synthetic air (not shown), a monotone decrease of the transmission and reflection behavior of the catalyst particles occurs especially during the first 120 min of time-on-stream, which is responsible for the systematic downward trend of the UV/Vis intensities at *ca.* 400 nm in the first part of the experiment. This may be due to coverage of catalyst particles with organic deposits on top of the catalyst bed near the dip of the glass-fiber optics. On the other hand, the systematic steps in the UV/Vis intensities at *ca.* 400 nm occurring simultaneously with switching off and on of the oxygen in the reactant flow (see Figs. 2 and 3, top) were found over the whole time-on-stream in a similar manner for three independent series of VPO/bulk and VPO/SBA-15 catalysts.

The *on-line* UV/Vis observation of the V^{5+} species was successfully utilized to control the completeness of the reduction and reoxidation of the catalysts before transferring them to the glove box. This application demonstrates the high potential of the glass-fiber UV/Vis spectroscopy for observing the oxidation state of VPO catalysts, which could be interesting for *on-line* measurements in industrial reactors.

For further XRD and solid-state NMR investigations of activated and reduced catalysts and of catalysts reoxidized after the first and fourth reduction period, samples were taken from the fixed-bed laboratory reactor at the times indicated with A, B, C, and D, respectively, in Figs. 2 and 3, top.

3.3. XRD characterization of VPO/bulk and VPO/SBA-15 catalyst samples prepared by sequential selective oxidation of n-butane

The catalyst samples taken at times A–D of the selective oxidation of *n*-butane (as assigned Figs. 2 and 3) were transferred in a glove box purged with dry nitrogen to XRD sample carriers and immediately covered and sealed by a gas-tight foil. With this treatment, no hydration of samples occurred during 48 h. Figs. 4 and 5 show the XRD patterns of the VPO/bulk and VPO/SBA-15 samples A–D from top to bottom, respectively.

According to literature [35], the main reflection lines of the vanadyl pyrophosphate $(VO)_2P_2O_7$ occur at 23.00°, 28.45°, and 29.95°. Therefore, reflection lines of $(VO)_2P_2O_7$ domains may contribute to the reflections at 28.5° and 30° in the XRD patterns in Figs. 4 and 5. In this case, the typical $(VO)_2P_2O_7$ reflection line at 23° causes the very broad reflection in the background in Fig. 4 and the broad hump in Fig. 5 at *ca.* 23°. The strong broadening of these reflections is a hint that the sizes of the corresponding crystalline $(VO)_2P_2O_7$ domains are in the order of the wavelength of the XRD radiation ($\lambda_{Cu,K\alpha}$ = 0.154 nm [36]). Because of the occurrence of additional reflection lines in Figs. 4 and 5, the corresponding patterns cannot be explained exclusively by $(VO)_2P_2O_7$ domains. Additional phases, which may contribute with their main reflection lines, are the var-

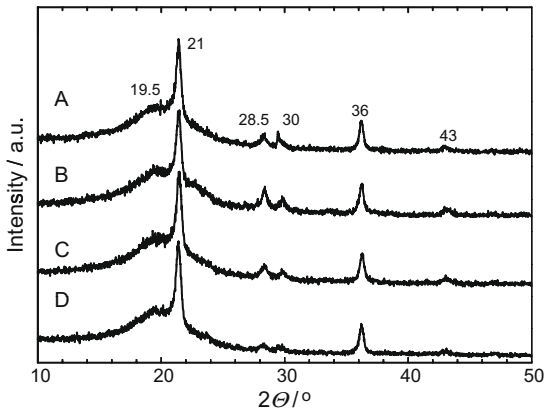

Fig. 4. XRD patterns of the VPO/bulk samples A–D as assigned in Fig. 2.

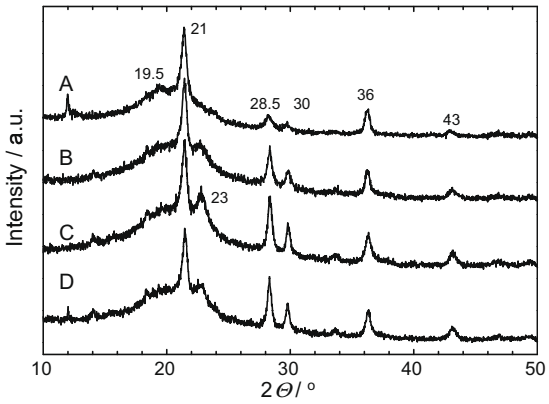

Fig. 5. XRD patterns of the VPO/SBA-15 samples A–D as assigned in Fig. 3.

ious orthophosphate phases (α_{II}-$VOPO_4$: 20.09°, 25.00°, 29.14° [35]; β-$VOPO_4$: 17.05°, 19.28°, 26.17°, 29.09° [35], for γ-$VOPO_4$ at 18.10°, 20,42°, 21.37°, 22.66°, 23.16°, 25.40°, 28.80°, 29.16°, and 36.61° [35]; δ-$VOPO_4$: 22.08°, 24.17°, 28.55°, 30.26°, 34.79°, 42.46° [35]). As evidenced by the reflection lines at *ca.* 19.5°, 21°, 36°, and 43° in Figs. 4 and 5, especially β-, γ-, and δ-$VOPO_4$ phases may contribute to the corresponding XRD patterns.

The most important changes in the XRD patterns of the VPO/bulk and VPO/SBA-15 catalysts comparing the samples A–D consists in a systematic decrease (Fig. 4) and increase (Fig. 5) of the reflections at 28.5° and 30°, respectively. There is no strong jump in the XRD line intensities for the samples B obtained after reduction of the VPO/bulk and VPO/SBA-15 catalysts. Hence, the reduction and reoxidation of the VPO/bulk and VPO/SBA-15 catalysts have no significant effect on the long-range order of their crystalline domains. The changes of the oxidation state of vanadium atoms ($V^{5+} \rightarrow V^{4+}$, V^{3+} and V^{4+}, $V^{3+} \rightarrow V^{5+}$) in the above-mentioned catalysts must be local effects, *e.g.* occurring on the surface of these crystalline domains, or are due to very small domains and amorphous compounds, both not accessible for X-ray diffraction methods.

3.4. Solid-state NMR investigation of VPO/bulk and VPO/SBA-15 catalysts prepared by sequential selective oxidation of n-butane

Important advantages of solid-state NMR spectroscopy are the high sensitivity for local structures and the quantitative character of this method. As already mentioned in Section 1, strong line broadenings and resonance shifts occur for the ^{31}P solid-state NMR signals of phosphorus atoms in the proximity of paramagnetic vanadium species (P/V^{3+} and P/V^{4+}) in VPO materials. On the other hand, highly resolved ^{31}P MAS NMR signals of four- and five-coordinated phosphorus atoms in various diamagnetic compounds are observed at *ca.* −100 to 100 ppm [37,38]). In the case of VPO materials, narrow ^{31}P MAS NMR signals appear exclusively for phosphorus atoms in the proximity of diamagnetic V^{5+} species (P/V^{5+}). In the present work, therefore, ^{31}P MAS NMR spectroscopy was utilized for the selective investigation of P/V^{5+} species in the VPO/bulk and VPO/SBA-15 catalysts causing characteristic signals at −40 to 10 ppm [20,24,35]. By an evaluation of the signal intensities, the changes in the number of P/V^{5+} species in result of the catalyst activation, reduction, and reoxidation were determined in a quantitative manner.

In Fig. 6, the ^{31}P MAS NMR spectra of the VPO/bulk samples A–D are depicted. The spectrum of sample A consists of a central line with a peak at −12 ppm and a shoulder at *ca.* −22 ppm due to P/V^{5+} species. Interestingly, these signals are absent in the spectrum of the completely reduced VPO/bulk sample B. This finding indicates a transformation of the former P/V^{5+} species in sample A into P/V^{4+} and possibly P/V^{3+} species in sample B, which cannot be observed in the spectral range under study. After reoxidation of the VPO/bulk catalyst leading to sample C, again ^{31}P MAS NMR signals occur at −12 to −22 ppm indicating that the former P/V^{4+} and P/V^{3+} species were reoxidized to P/V^{5+} species. Also in the spectrum of the VPO/bulk sample D, which was obtained after four reduction and reoxidation cycles, signals occur at −12 to −22 ppm. Considering the chemical shifts of the ^{31}P MAS NMR signals caused by the various vanadyl orthophosphate phases, the central line of the VPO/bulk catalysts in Fig. 6 may be due to a composition of α_{II}-$VOPO_4$ (−20.5 ppm), β-$VOPO_4$(−11.5 ppm), γ-$VOPO_4$ (−21.2 and −17.3 ppm), and δ-$VOPO_4$ (−17.6 and −8.4 ppm) [24,35]. Because of the limited resolution, however, no detailed assignment of the ^{31}P MAS NMR signals was possible.

In the further step, the number of phosphorus atoms in P/V^{5+} species as obtained by a quantitative evaluation of the integral ^{31}P MAS NMR intensities in Fig. 6 was compared with the total number of phosphorus atoms in the VPO/bulk catalyst as determined by ICP-AES. The corresponding data are summarized in Table 3. According to these values, only 0.5% of all phosphorus atoms in the activated VPO/bulk sample A exist in the proximity of V^{5+}

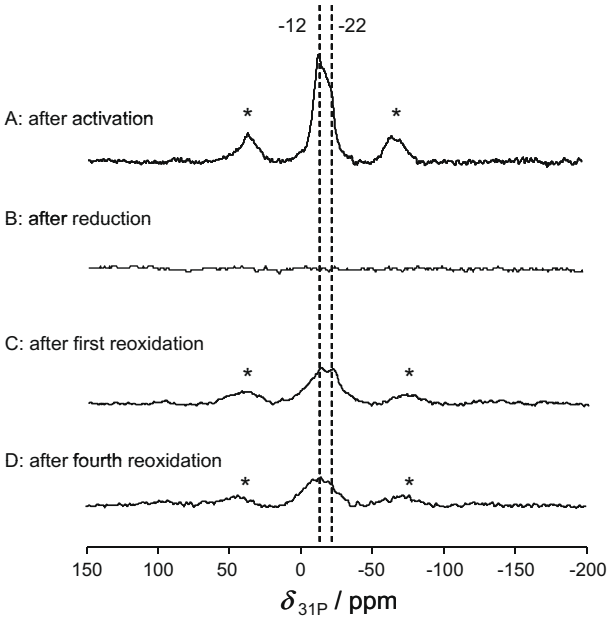

Fig. 6. ^{31}P MAS NMR spectra of the VPO/bulk samples A–D as assigned in Fig. 2. Asterisks denote spinning sidebands.

species. After reduction of the VPO/bulk catalyst, there is a total decline of these species, while they appear again with a content of 0.3–0.4% of all phosphorus atoms after the reoxidation procedure (samples C and D).

Like for the VPO/bulk catalysts, also the ^{31}P MAS NMR signals of the VPO/SBA-15 samples A–D occur in the shift range of −12 to −22 ppm, but with a significantly better signal-to-noise ratio and spectral resolution (Fig. 7). In addition, there is a broad signal at *ca.* −38 ppm due to phosphorus atoms bound to silicon atoms of the SBA-15 support *via* oxygen bridges (P/SiO_2) [20]. The quantitative evaluation of the ^{31}P MAS NMR spectra of the VPO/SBA-15 samples A–D (see Table 3) led to significantly higher contents of phosphorus atoms in P/V^{5+} species in comparison with the VPO/bulk catalysts treated in the comparable manner. While in the VPO/bulk sample A only 0.5% of all phosphorus atoms exist in P/V^{5+} species, the content of 2.6% for the phosphorus atoms in P/V^{5+} and P/SiO_2 species in the VPO/SBA-15 sample A was determined, which goes down to 0.3% for the reduced sample B. In the reoxidized VPO/SBA-15 samples C and D, 0.9–1.3% of the phosphorus atoms exist as P/V^{5+} and P/SiO_2 species. The much stronger signals of P/V^{5+} species in the spectra of VPO/SBA-15 catalysts may be due to the larger specific surface area of the well-dispersed VPO compounds in this material in comparison with the VPO/bulk catalyst. This finding makes VPO compounds supported on SBA-15 material to interesting model catalysts for spectroscopic studies.

^{51}V MAS NMR spectroscopy of vanadium atoms existing as V^{5+} species is a further approach for the investigation of the catalytically interesting VPO compounds. Numerous investigations on diamagnetic V^{5+} species in solids were published [21–23]. Although ^{51}V nuclei have a spin $I = 7/2$, *i.e.* are quadrupolar nuclei, the anisotropic chemical shielding is the strongest line broadening mechanism, since the quadrupolar coupling constant reaches values of maximum $C_Q = 2$ MHz only [21–23].

The ^{51}V MAS NMR spectra of the VPO/SBA-15 samples A–D in Fig. 8 were recorded with sample spinning rates of 12.5 and 20.0 kHz to allow an assignment of the central lines (equal position for different sample spinning rates). In most spectra, signals with isotropic chemical shifts of −735 and −765 to 775 ppm occur. While the signals at −735 ppm dominates the spectra of the VPO/SBA-15 sample A, this signal disappears in the spectra of sample B and appears again as weak signals in the spectra of samples C and D. The signal at *ca.* −770 ppm exists also in the spectra of the completely reduced sample B and shows a weak increase in the spectra of samples C and D. The broad sideband patterns of the ^{51}V MAS NMR spectra and the resulting low signal-to-noise ratio of the central line hindered their quantitative evaluation. The qualitative comparison of the ^{51}V MAS NMR spectra of the VPO/SBA-15 samples A–D, on the other hand, indicates a strong decrease of the signal intensities upon reduction of the activated catalyst (sample A → sample B) and a significant increase of the intensities after reoxidation (sample B → sample C and sample D). Hence, the changes in the total intensities of the ^{51}V MAS NMR signals are comparable with the intensity changes observed for the corresponding ^{31}P MAS NMR spectra.

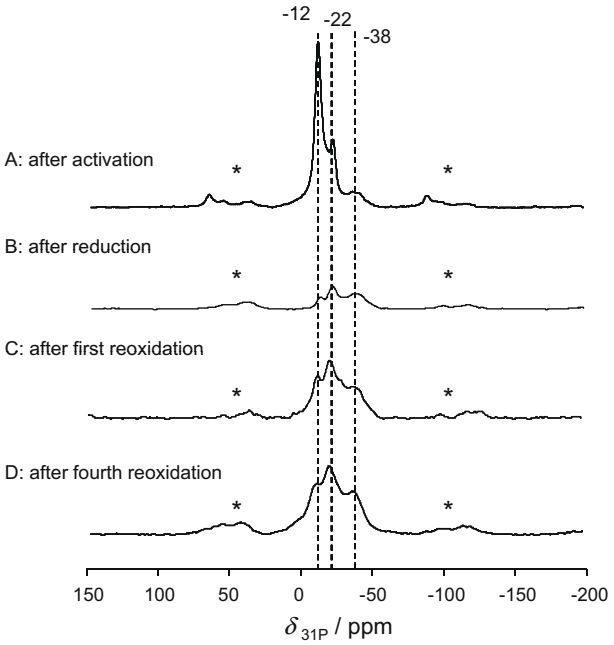

Fig. 7. ^{31}P MAS NMR spectra of the VPO/SBA-15 samples A–D as assigned in Fig. 3. Asterisks denote spinning sidebands.

Previous investigations on $VOPO_4$ reference materials support the assignment of the signals at −735 and −770 ± 5 ppm [21–23]. According to these studies, the α_{II}-$VOPO_4$ phase causes ^{51}V MAS NMR signals with isotropic chemical shifts of −755 and −776 ppm explaining the high-field signals in the spectra of Fig. 8. The signal at −735 ppm may be due to β-$VOPO_4$ (−735 ppm) and γ-$VOPO_4$ (−739 ppm). However, it must be mentioned that no reference data exist for the δ-$VOPO_4$ and, therefore, a contribution also of this phase cannot be excluded.

Table 3
Contents of phosphorus atoms in P/V^{5+} and P/SiO_2 species in the VPO/bulk and VPO/SBA-15 samples A–D as determined by quantitative evaluation of the ^{31}P MAS NMR spectra in Figs. 6 and 7.

Material	Treatment	Contents of P/V^{5+} and P/SiO_2[a] (%)	Contents of P/V^{5+} in δ-$VOPO_4$-like phases[b] (%)
VPO/bulk	A	0.5	
	B	0	
	C	0.35	
	D	0.4	
VPO/SBA-15	A	2.6	0.80
	B	0.3	0.05
	C	0.9	0.20
	D	1.3	0.30

[a] Contents of phosphorus atoms causing signals at chemical shifts of −40 to 10 ppm, *i.e.*, in the vicinity of V^{5+} species (P/V^{5+}) and on the SBA-15 support (P/SiO_2), accuracy ± 10%.

[b] Contents of phosphorus atoms causing signals at chemical shifts of −8 ± 1 and −18 ± 1 ppm, *i.e.*, exclusively of phosphorus atoms in the vicinity of V^{5+} species contributing to δ-$VOPO_4$-like phases, accuracy ±10%.

3.5. Solid-state NMR characterization of surface species on the VPO/SBA-15 catalyst

The observation, that the ^{31}P MAS NMR signals of phosphorus atoms in P/V^{5+} species and the ^{51}V MAS NMR signals of the corresponding V^{5+} atoms are strongly influenced by the reduction and reoxidation treatments of the VPO catalysts, is a hint that these species exist in surface-near regions of the particles. A further support for their surface-near location was obtained by ^{31}P{^{1}H} cross-polarization MAS NMR studies of the VPO/SBA-15 sample C without and after loading with *n*-butane (Fig. 9). In this cross-polarization (CP) experiments, the ^{1}H nuclei of surface compounds, such as adsorbate molecules and hydroxyl protons, are excited *via* a $\pi/2$ pulse. Subsequently, the produced polarization is transferred from the ^{1}H nuclei to dipolarly coupled ^{31}P nuclei in the surface-near region of the catalyst particles. Finally, the ^{31}P MAS NMR signal of these dipolarly coupled ^{31}P nuclei is recorded.

The very weak signals in ^{31}P{^{1}H} CPMAS NMR spectrum of unloaded VPO/SBA-15 sample C (Fig. 9a) are due to a polarization

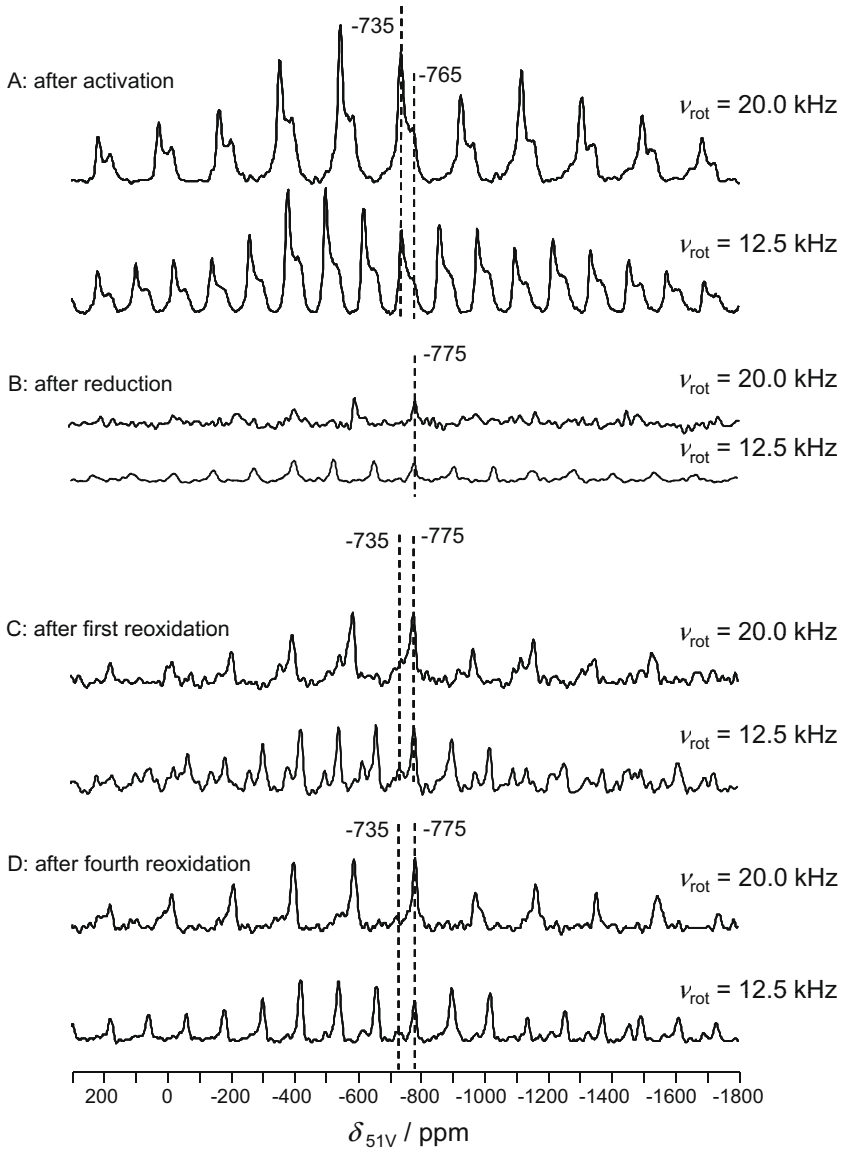

Fig. 8. ^{51}V MAS NMR spectra of VPO/SBA-15 samples A–D as assigned in Fig. 3 and each recorded at sample spinning rates of 20.0 kHz (top) and 12.5 kHz (bottom).

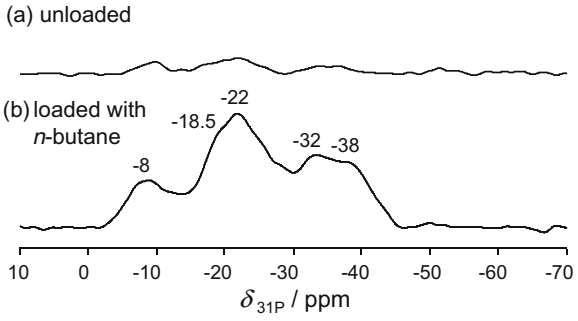

Fig. 9. ^{31}P{^{1}H} cross-polarization MAS NMR spectra (CPMAS NMR) of the VPO/SBA-15 sample C recorded before (a) and after (b) loading with 200 mbar *n*-butane, both recorded with 4800 scans.

transfer between the ^{1}H nuclei of surface hydroxyl groups (POH) and neighboring ^{31}P nuclei in the VPO framework. After loading the VPO/SBA-15 sample C with 200 mbar *n*-butane (Fig. 9b), a strong increase of the ^{31}P{^{1}H} CPMAS NMR signals occurred. This finding indicates that ^{1}H nuclei in adsorbed *n*-butane molecules contribute to the polarization transfer causing the significant enhancement of the ^{31}P{^{1}H} CPMAS NMR signals. The corresponding phosphorus atoms must be located in the local structure of the adsorption sites, *i.e.* in the surface-near region of the VPO compounds. Interestingly, the low-field signal in the spectrum of Fig. 9b occurs at −8 ppm and not at −12 ppm like in the spectra of Fig. 7. In addition, the signal at −21 ppm has a significant shoulder at −18.5 ppm. Both these signals at −8 and −18.5 ppm are hints to a preferred adsorption of *n*-butane at surface site of orthophosphate phases with a structure similar to δ-$VOPO_4$ (−17.6 and −8.4 ppm) [35]).

The ^{31}P{^{1}H} CPMAS NMR experiments indicate that P/V^{5+} species in orthophosphate phases with a structure similar to δ-$VOPO_4$ play a role as surface sites of the VPO/SBA-15 catalyst. Therefore, the central lines in the ^{31}P MAS NMR spectra of the VPO/SBA-15 samples A–D in Fig. 8 were simulated using signals of δ-$VOPO_4$-like phases at −8 and −18 ppm [35], β-$VOPO_4$ at −12 ppm [35], α_{II}-$VOPO_4$ at −22 ppm [35], and two signals of phosphorus atoms bound to the SBA-15 support (P/SiO_2) at −27 and −38 ppm [20]

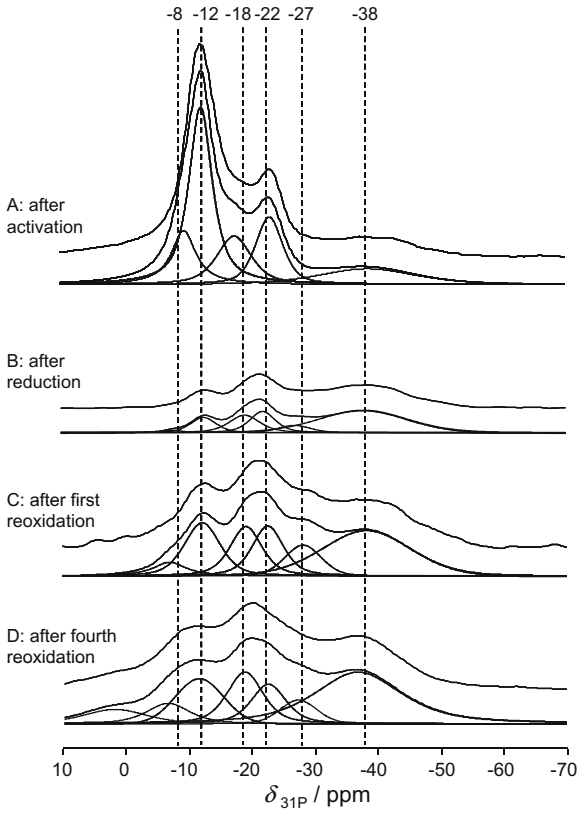

Fig. 10. Decomposition and simulation of the ^{31}P MAS NMR central lines of the VPO/SBA-15 samples A–D from top to bottom.

(see Fig. 10). The obtained contents of phosphorus atoms contributing to P/V^{5+} species in δ-VOPO$_4$-like phases are given in Table 3, last column. These values change in a characteristic manner with the reduction and reoxidation treatment.

According to the contents of phosphorus atoms in P/V^{5+} species of δ-VOPO$_4$-like phases (Table 3, last column), *ca.* 0.2% of all vanadium atoms may contribute to the oxidation reaction catalyzed by the VPO/SBA-15 material. Due to the selectivity to maleic anhydride of *ca.* 50%, only *ca.* 50% of the above-mentioned species catalyze the reaction to the desired product. In this case, the *n*-butane conversion of 36% and the selectivity to maleic anhydride of 45% (Table 2) lead to the turnover frequency of 0.186 s^{-1} for the P/V^{5+} species exclusively active in the maleic anhydride formation. The selective oxidation of one *n*-butane molecule requires the release of four oxygen atoms from the catalyst framework for the dehydrogenation of *n*-butane to butadiene and of three oxygen atoms for the oxidation of butadiene to maleic anhydride. The very complex 'surface sites' catalyzing the selective oxidation of *n*-butane to maleic anhydride, therefore, must consist of seven P/V^{5+} species at the catalyst surface, which must be reduced and reoxidized at least with the above-mentioned turnover frequency of about 0.2 s^{-1}.

Considering the low resolution of the ^{31}P MAS NMR spectra, future investigations are required for supporting the solid-state NMR evidence for the active role of V^{5+} species in δ-VOPO$_4$-like phases in the selective oxidation of *n*-butane to maleic anhydride.

4. Conclusions

Sequential selective oxidation of *n*-butane to maleic anhydride was performed by switching off and on the oxygen flow in the feed, which led to a complete reduction and reoxidation, respectively, of the VPO/bulk and VPO/SBA-15 catalysts under study. The complete reduction and reoxidation of the VPO materials were observed *on-line* by fiber-optic UV/Vis spectroscopy *via* the charge-transfer band of V^{5+} species occurring at *ca.* 400 nm.

After transferring the activated, reduced, and reoxidized VPO/bulk and VPO/SBA-15 catalysts into MAS NMR rotors, quantitative *ex situ* solid-state NMR investigations indicated that maximum 0.5–2.3% of the total number of phosphorus atoms contribute to P/V^{5+} species contribute to oxidation reactions catalyzed by the VPO materials under study.

By ^{31}P{^{1}H} cross-polarization MAS NMR experiments on the VPO/SBA-15 catalyst loaded with *n*-butane was demonstrated that most of the above-mentioned P/V^{5+} species are located in a surface-near region. Furthermore, a preferred adsorption of *n*-butane at orthophosphate phases with δ-VOPO$_4$-like structure was found. The number of P/V^{5+} species in these orthophosphate phases with δ-VOPO$_4$-like structure correlates well with the reduction and reoxidation cycle of the VPO/SBA-15 catalyst.

Based on the *n*-butane conversion and the selectivity to maleic anhydride reached on the VPO/SBA-15 catalyst and the number of active P/V^{5+} species in δ-VOPO$_4$ phases as determined by quantitative ^{31}P MAS NMR spectroscopy, the turnover frequency of these sites was estimated to about 0.2 s^{-1}.

In future investigations, solid-state NMR spectroscopy of spent oxidation catalysts is planned to combine with surface-sensitive analytical methods, such as Raman spectroscopy, in one equipment. This approach would be useful for comparing the state of the catalyst samples under *in situ* and *ex situ* conditions. Until now, however, *in situ* solid-state NMR spectroscopic investigations of VPO catalysts during the selective oxidation of alkanes are hindered due to the required reaction temperature and the low content of P/V^{5+} species in the activated catalyst samples as estimated in the present study.

Acknowledgments

Financial support of this project by Deutsche Forschungsgemeinschaft (HU533/9-2) and Fonds der Chemischen Industrie is gratefully acknowledged.

References

[1] J.K. Bartley, N.F. Dummer, G.J. Hutchings, in: S.D. Jackson, J.S.J. Hargreaves (Eds.), Metal Oxide Catalysis, vol. 2, Wiley-VCH, Weinheim, 2009, pp. 499–537.
[2] T. Okuhara, M. Misono, Catal. Today 16 (1993) 61–67.
[3] E. Bordes, Catal. Today 16 (1993) 27–37.
[4] Y. Zhang, R.P.A. Sneeden, J.C. Volta, Catal. Today 16 (1993) 39–49.
[5] V.V. Guliants, J.B. Benzinger, S. Sundaresan, I.E. Wachs, J.-M. Jehng, J.E. Roberts, Catal. Lett. 32 (1995) 379–386.
[6] G.J. Hutchings, C.J. Kiely, M.T. Sanchez-Schulz, A. Burrows, J.C. Volta, Catal. Today 40 (1998) 273–286.
[7] G. Koyano, T. Okuhara, M. Misono, J. Am. Chem. Soc. 120 (1998) 767–774.
[8] M. Hävecker, R.W. Mayer, A. Knop-Gericke, H. Bluhm, E. Kleimenov, A. Liskowski, D. Su, R. Follath, F.G. Requejo, D.F. Ogletree, M. Salmeron, J.A. Lopez-Sanchez, J.K. Bartley, G.J. Hutchings, R. Schlögl, J. Phys. Chem. B 107 (2003) 4587–4596.
[9] H. Bluhm, M. Hävecker, E. Kleimenov, A. Knop-Gericke, A. Liskowski, R. Schlögl, D.S. Su, Top. Catal. 23 (2003) 99–107.
[10] E. Kleimenov, H. Bluhm, M. Hävecker, A. Knop-Gericke, A. Pestryakov, D. Teschner, J.A. Lopez-Sanchez, J.K. Bartley, G.J. Hutchings, R. Schlögl, Surf. Sci. 575 (2005) 181–188.
[11] M. Conte, G. Budroni, J.K. Bartley, S.H. Taylor, A.F. Carley, A. Schmidt, D.M. Murphy, F. Girgsdies, T. Ressler, R. Schlögl, G.J. Hutchings, Science 313 (2006) 1270–1273.
[12] G. Centi, Catal. Today 16 (1993) 5–26.
[13] G.J. Hutchings, A. Desmartin-Chomel, R. Oller, J.-C. Volta, Nature 368 (1994) 41–45.
[14] C.J. Kiely, A. Burrows, S. Sajip, G.J. Hutchings, M.T. Sananes, A. Tuel, J.-C. Volta, J. Catal. 162 (1996) 31–47.
[15] C.J. Kiely, G.J. Hutchings, Appl. Catal. A: General 325 (2007) 194–197.
[16] G. Ertl, H. Knözinger, F. Schüth, J. Weitkamp, Handbook of Heterogeneous Catalysis, second ed., Wiley-VCH, Weinheim, 2008. p. 3963.
[17] J. Li, M.E. Lashier, G.L. Schrader, B.C. Gerstein, Appl. Catal. 73 (1991) 83–95.

[18] M.T. Sananes-Schulz, A. Tuel, G.J. Hutchings, J.C. Volta, J. Catal. 166 (1997) 388–392.
[19] M.T. Sananes, A. Tuel, Solid State Nucl. Magn. Reson. 6 (1996) 157–166.
[20] K.E. Birkeland, S.M. Babitz, G.K. Bethke, H.H. Kung, G.W. Coulston, S.R. Bare, J. Phys. Chem. B 101 (1997) 6895–6902.
[21] O.B. Lapina, D.F. Khabibulin, A.A. Shubin, V.M. Bondareva, J. Mol. Catal. A: Chem. 162 (2000) 381–390.
[22] R. Siegel, N. Dupre, M. Quarton, J. Hirschinger, Mag. Res. Chem. 42 (2004) 1022–1026.
[23] O.B. Lapina, D.F. Khabibulin, A.A. Shubin, V.V. Terskikh, Progr. Nucl. Magn. Reson. Spetrosc. 53 (2008) 128–191.
[24] J. Frey, Y.S. Ooi, B. Thomas, V.R. Reddy Marthala, A. Bressel, T. Schoelkopf, T. Schleid, M. Hunger, Solid State Nucl. Magn. Reson. 35 (2009) 130–137.
[25] X.-K. Li, W.-J. Ji, J. Zhao, Z.-B. Zhang, C.-T. Au, J. Catal. 238 (2006) 232–241.
[26] X.-K. Li, W.-J. Ji, J. Zhao, Z.-B. Zhang, C.-T. Au, Appl. Catal. A: General 306 (2006) 8–16.
[27] H.S. Horowitz, C.M. Blackstone, A.W. Sleight, G. Teufer, Appl. Catal. 38 (1988) 193–210.
[28] G.J. Hutchings, J. Mater. Chem. 14 (2004) 3385–3395.
[29] D.Y. Zhao, J.L. Feng, Q.S. Huo, N. Melosh, G.H. Friedrickson, B.F. Chmelka, G.D. Stucky, Science 279 (1998) 548–552.
[30] B.M. Weckhuysen, Phys. Chem. Chem. Phys. 5 (2003) 4351–4360.
[31] Y. Jiang, J. Huang, J. Weitkamp, M. Hunger, Stud. Surf. Sci. Catal., vol. 170, Elsevier, Amsterdam, 2007. pp. 1137–1144.
[33] J.W. Niemantsverdriet, Spectroscopy in Catalysis, VCH, Weinheim, 1995. p. 200.
[32] G. Bignardi, F. Cavani, C. Cortelli, T. De Lucia, F. Pierelli, F. Trifiro, G. Mazzoni, C. Fumagalli, T. Monti, J. Mol. Catal. A: Chem. 244 (2006) 244–251.
[34] A. Buchholz, W. Wang, M. Xu, A. Arnold, M. Hunger, Micropor. Mesopor. Mater. 56 (2002) 267–278.
[35] F.B. Abdelouhab, R. Olier, N. Guilhaume, F. Lefebvre, J.C. Volta, J. Catal. 134 (1992) 151–167.
[36] H.-J. Bautsch, J. Bohm, I. Kleber, Einführung in die Kristallographie, Verlag Technik GmbH, Berlin, 1990. p. 334.
[37] K.R. Dixon, in: J. Mason (Ed.), Multinuclear NMR, Plenum Press, New York, 1987. p. 369.
[38] M. Hunger, E. Brunner, Molecular sieves, in: H.G. Karge, J. Weitkamp (Eds.), Characterization I, vol. 4, Springer-Verlag, Berlin, 2004, p. 231.